

MATERIALS SCIENCE

Flexible active-matrix organic light-emitting diode display enabled by MoS₂ thin-film transistorMinwoo Choi,^{1*} Yong Ju Park,^{1*} Bhupendra K. Sharma,¹ Sa-Rang Bae,² Soo Young Kim,^{2†} Jong-Hyun Ahn^{1†}

Atomically thin molybdenum disulfide (MoS₂) has been extensively investigated in semiconductor electronics but has not been applied in a backplane circuitry of organic light-emitting diode (OLED) display. Its applicability as an active drive element is hampered by the large contact resistance at the metal/MoS₂ interface, which hinders the transport of carriers at the dielectric surface, which in turn considerably deteriorates the mobility. Modified switching device architecture is proposed for efficiently exploiting the high-*k* dielectric Al₂O₃ layer, which, when integrated in an active matrix, can drive the ultrathin OLED display even in dynamic folding states. The proposed architecture exhibits 28 times increase in mobility compared to a normal back-gated thin-film transistor, and its potential as a wearable display attached to a human wrist is demonstrated.

INTRODUCTION

Recently, to realize intelligent electronic systems, there is an increasing demand to combine functional features such as ultrathin characteristics (1, 2), large area (3), wrapping onto irregular surfaces (4, 5), easy attachment to the human body (6, 7), and several other characteristics (8, 9) with the current electronic circuitry. Compared to other typically investigated organic (10, 11) and inorganic materials (12), van der Waals materials with atomic thickness demonstrate the immense potential for these systems (13). Transition metal dichalcogenides such as MoS₂ and WSe₂ with a two-dimensional (2D) atomic layer have been reported to be superior to conventional materials owing to their exceptional electrical and mechanical properties (14–16). On the basis of their outstanding properties, these materials can be exploited for large-area flexible switching-based applications. In particular, the active-matrix backplane for flexible organic light-emitting diode (OLED) displays is one of the most promising applications of these 2D semiconductors because they offer important benefits such as high carrier mobility, high optical transmittance, and low flexural rigidity required for switching OLEDs on a flexible substrate compared to conventional inorganic semiconductors. Although a few studies have demonstrated the switching of a single-pixel OLED using mechanically exfoliated 2D materials as the semiconducting channel of a thin-film transistor (TFT) (17, 18), these capabilities have not been investigated in flexible systems or in the active-matrix backplane circuitry for large-area OLED displays. Exfoliated monolayer MoS₂ exhibits excellent field-effect mobility (10 to 40 cm² V⁻¹ s⁻¹), but it is not a suitable method for real electronic applications (10). Large-area MoS₂ films prepared using chemical vapor deposition (CVD) have been considered as a more favorable candidate for OLED displays, although they exhibit low mobility that results from small grain size, inherently rendering its semiconducting features inferior to those of the exfoliated materials (19). However, MoS₂ as an active channel material has serious drawbacks including the large contact barrier between the source/drain (S/D) metal electrode and MoS₂ channel and the electron transport hindered by Coulomb scattering and trap charges at the interface between the

gate dielectric and MoS₂ in the TFT configuration, in comparison with conventional inorganic semiconductors (20). These factors significantly reduce the mobility of MoS₂-based TFTs to ≤ 1 cm² V⁻¹ s⁻¹, which is comparable to that of a-H Si (21). This low-mobility value prohibits the integration of MoS₂ TFTs into large-area active-matrix OLED (AM-OLED) displays (22–24). Although researchers have attempted to improve the carrier mobility of devices by integrating high-*k* dielectric materials such as Al₂O₃ or HfO₂ as a gate dielectric in a conventional manner, there are still significant challenges in satisfying the electrical specification demands of various electronic applications (25–27).

Here, a TFT device is designed using the Al₂O₃ layer in various ways. This Al₂O₃-capped TFT device leads to reduced contact resistance at the metal/MoS₂ interface and permits the doping of the channel region, which, in turn, reduces the scattering charge impurities and an effective decrease in the interface-trapped charge density via a smooth surface. All these benefits synergistically yield uniform MoS₂ TFT arrays with high mobility, which can efficiently operate OLED pixels on flexible plastic substrates.

RESULTS

The backplane circuitry of a flexible display, comprising an array of transistors responsible for turning the individual OLED pixels ON and OFF, was fabricated using a metal-organic CVD (MOCVD)-grown bilayer MoS₂ film on a 6- μ m-thick ultrathin polyethylene terephthalate (PET) substrate (Fig. 1A). The MoS₂ TFT has a top-gate configuration sandwiched between two high-*k* dielectric Al₂O₃ layers, leading to the enhancement of the carrier mobility because the top dielectric Al₂O₃ layer facilitates the doping of the MoS₂ film at the channel and S/D contact regions. Furthermore, the bottom Al₂O₃ layer on the SiO₂/Si substrate reduces the roughness and provides a smooth substrate surface compared with that of bare SiO₂ (Fig. 1B). In particular, in contrast to the conventional device structure of MoS₂ TFTs, in which the S/D electrodes are formed on top of the MoS₂ film, the S/D electrodes of the device are located below the MoS₂ film, which aids the subsequent deposition of the top dielectric Al₂O₃ layer and effectively reduces the contact resistance of the S/D contact regions. The decrease in contact resistance enhances the carrier mobility and facilitates the OLED display operation, which requires a high amount of current (28). In the atomic force microscopy and cross-sectional high-resolution

Copyright © 2018
The Authors, some
rights reserved;
exclusive licensee
American Association
for the Advancement
of Science. No claim to
original U.S. Government
Works. Distributed
under a Creative
Commons Attribution
NonCommercial
License 4.0 (CC BY-NC).

¹School of Electrical and Electronic Engineering, Yonsei University, Seoul 03722, Republic of Korea. ²School of Chemical Engineering and Materials Science, Chung-Ang University, Seoul 06974, Republic of Korea.

*These authors contributed equally to this work.

†Corresponding author. Email: sooyoungkim@cau.ac.kr (S.Y.K.); ahnj@yonsei.ac.kr (J.-H.A.)

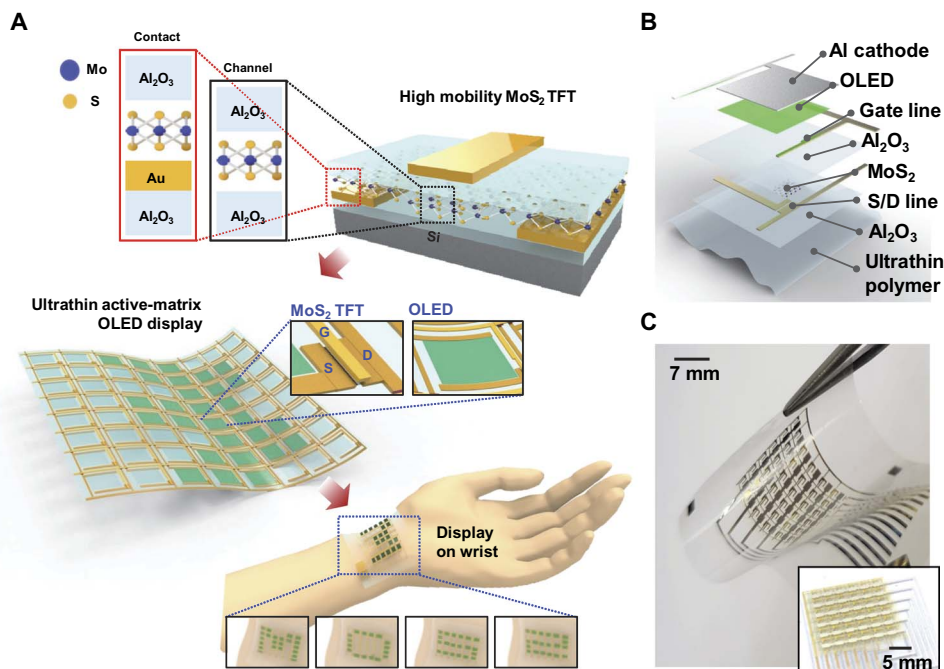


Fig. 1. The device structure of flexible OLED display with MoS₂-based backplane circuitry. (A) Schematic of high-mobility MoS₂ TFT using an Al₂O₃ passivation layer. The Al₂O₃ passivation layer ensures n-type doping of not only the MoS₂ channel region but also the contact region (top); ultrathin AM-OLED display using the high-performance MoS₂-based backplane array (middle), which is attached as a display to human skin (bottom). (B) Specific layer structure of the ultrathin AM-OLED display. The thickness of the total display system is less than 7 μm. (C) Optical image of the assembled display on the flexible ultrathin polymer substrate; low bending stiffness of the display offers ultraflexibility. The inset image shows the flat state of the active-matrix display circuit.

transmission electron microscopy images, improved surface roughness and conformal attachment of the MoS₂ film to the top and bottom Al₂O₃ layers were observed, indicating a clean interface without pinholes or gaps (figs. S1 and S2). The OLED display driven by the bilayer MoS₂-based backplane TFTs was well operated even under bent status or when attached to a human wrist, indicating the possible applications to wearable displays (Fig. 1, A and C) (28).

It is crucial to explain the mechanism by which the carrier mobility of bilayer MoS₂ TFTs increases with the use of two dielectric Al₂O₃ layers. The high-*k* Al₂O₃ layer facilitates considerable n-type doping of the MoS₂ layer owing to its oxygen-deficient surface. From earlier studies, band structure calculations have indicated that the presence of interfacial oxygen vacancies in the Al₂O₃ layer lowers the conduction band edge below the Fermi level and initiates the filling of the lower conduction band states of MoS₂ at the interface, leading to the n-type carrier injection in MoS₂ (25). Moreover, the large dielectric mismatch at the Al₂O₃/MoS₂ interface suppresses the Coulombic impurities effectively in the MoS₂ layer (26). These benefits associated with the presence of a high-*k* dielectric environment possibly enhance the carrier mobility of the resultant MoS₂ TFTs (27). The additional advantage of the modified TFT structure is rendered by the bottom Al₂O₃ layer, which provides low surface roughness and further improves the device performance via the suppression of the interface-trapped charge density. The n-type doping owing to the top Al₂O₃ layer in the proposed structure is evident from the Raman and photoluminescence spectra of the bilayer MoS₂ film with different combinations of Al₂O₃ as compared to the bare SiO₂/Si substrate (figs. S3 to S5 and see the Supplementary Materials).

In addition to the damping of the Coulomb scattering and suppression of the interface trap charges, the top Al₂O₃ layer is used for doping

MoS₂ in the channel and contact regions in our modified TFT structure. The increased electron concentration at the S/D contact regions reduces the Schottky barrier width, significantly decreasing the contact resistance R_c (fig. S6) (29). The decrease in R_c in combination with the doped channel, damped Coulomb scattering, and low surface roughness results in an increase of carrier mobility and uniform output characteristics of the MoS₂ TFTs on a large-area substrate.

To clarify the effect of the top and bottom Al₂O₃ layers to MoS₂ TFT, the devices with each layer and both layers are prepared using MOCVD-grown MoS₂ film (Fig. 2A and table S1). It is evident that back-gate dc characteristics of TFT fabricated on bare SiO₂/Si wafer exhibited a significant improvement in the ON current (②) after Al₂O₃ layer encapsulation, which confirms the doping effect owing to the top Al₂O₃ layer (Fig. 2A). In case of the top gate, a slight increment in the ON current (③) was observed, compared to the back-gate, encapsulated TFT (②), and this increment was further improved (④) for the channel sandwiched between the top and bottom Al₂O₃ layers (Fig. 2A). Here, the bottom Al₂O₃ layer in the sandwiched channel plays a crucial role in reducing the hysteresis significantly owing to the reduction in interface trap charge density (fig. S7 and see the Supplementary Materials). These improved features were also evident in output characteristics and mobility enhancement: a significant boost-up in mobility value (~28 times), positive threshold voltage, V_{th} (~5 V), high ON/OFF ratio (~10⁸), and transconductance (1.2×10^{-7} S μm⁻²) as compared to conventional back-gate structure (Fig. 2, B and C, fig. S8, and table S1). In particular, the positive V_{th} of top-gated TFT can maintain the OFF state of the pixel without the supply of an additional gate bias voltage, which consequently reduces the unnecessary power consumption during the selective pixel operation (table S1). Moreover, there have also been similar effects with MoS₂ single crystal (fig. S9) (30, 31). Thus,

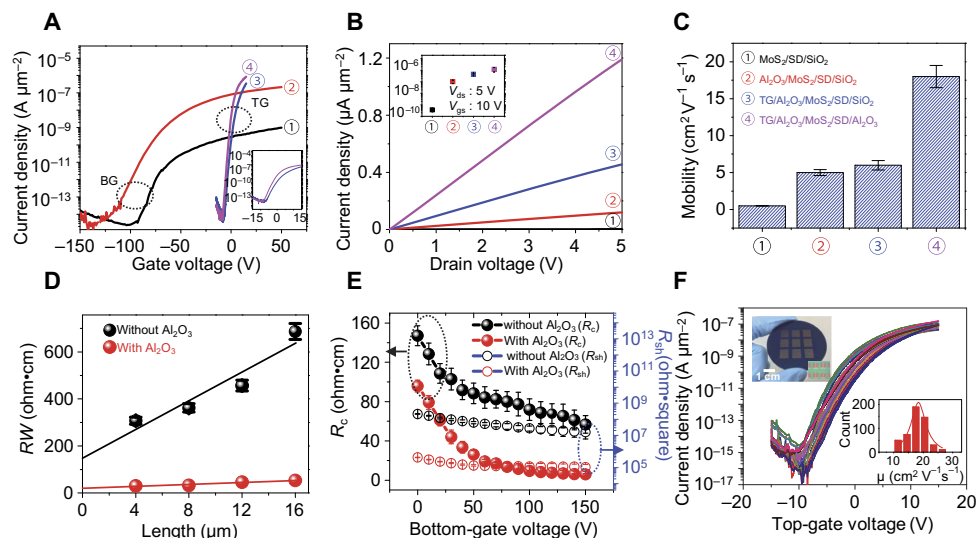


Fig. 2. The device characteristics of MoS₂ TFTs with different structures. (A) Transfer characteristics of bilayer MoS₂ TFTs with various device structures (in all cases, MoS₂ was on top of S/D contacts); [inset shows the top-gated (TG) ③ and ④] back-gated (BG) MoS₂ TFT on SiO₂/Si (①), back-gated MoS₂ TFT on SiO₂/Si with Al₂O₃ encapsulation (②), top-gated MoS₂ TFT on SiO₂/Si (③), and top-gated MoS₂ TFT on Al₂O₃/SiO₂/Si (④). The top-gated MoS₂ TFT sandwiched by two Al₂O₃ layers (④) showed the high performance over other fabricated TFTs. (B) Output characteristics of all TFTs (①, ②, ③, and ④) corresponding to (A); inset shows the increment of current density at shown bias. (C) Mobility values for all TFTs (①, ②, ③, and ④) corresponding to (A). (D) Transfer line plot for extracting line contact resistivity (R_c) and channel sheet resistance (R_{sh}) under different gating conditions. (E) Extracted R_c (filled circle) and R_{sh} (empty circle) of back-gated bilayer MoS₂ TFTs on Al₂O₃/SiO₂ substrate before (black) and after (red) Al₂O₃ deposition. (F) Transfer characteristics of top-gated Al₂O₃/MoS₂/Al₂O₃ sandwiched TFTs (100 devices). Insets show the photograph of wafer-scale fabrication of TFTs and mobility histogram for 500 TFTs showing the average value of mobility (18.1 cm² V⁻¹ s⁻¹).

these characteristics of devices show enough performance capabilities to satisfy the needs of TFT for the operation of the OLED display.

The values of R_c and channel sheet resistance (R_{sh}), which are the important factors influencing the mobility, must be estimated at the S/D/MoS₂ contact region and the MoS₂ channel between the S/D metal electrodes, respectively. The contact properties were characterized as the back-gate dc characteristics of TFTs with and without Al₂O₃ encapsulation. The transfer length method was performed to quantify R_c using TFTs fabricated for the channel lengths of 4, 8, 12, and 16 μm (see the Supplementary Materials). The R_c value, which was calculated as the intercept from the linear fitting of the RW (R , total measured resistance; W , channel width) plot against channel lengths, was 5.9 ± 0.7 ohm-cm and 56.7 ± 9.1 ohm-cm (at $V_{gs} = 150$ V; $V_{ds} = 1$ V) for TFTs with and without the Al₂O₃ encapsulation, respectively (Fig. 2D). The R_c value decreased with the increase in the back-gate voltage owing to the electrical doping of MoS₂ with applied gate bias, which reduced the effective barrier height (Fig. 2E) (32). R_{sh} remained almost unchanged with the application of back-gate voltages (Fig. 2E); however, a small decrement was observed owing to the increased carrier concentration near the accumulated region for channel formation. In case of top-gate TFTs, there were no significant changes observed in the values of R_c and R_{sh} as compared to back-gate TFTs (Fig. 2E and fig. S10). Notably, R_c and R_{sh} are reduced owing to the presence of the top Al₂O₃-encapsulated layer, leading to significant improvement in the mobility. The above experimental results demonstrate that the top Al₂O₃ dielectric layer effectively doped MoS₂ in both the channel and overlapped contact regions. The doping in the channel region increased the effective carrier concentration, leading to the improved ON current and negative shift in V_{th} , whereas the increased concentration of electrons at the contact region reduced the metal/MoS₂ barrier width, thereby considerably decreasing the values of R_c . Therefore, the improvement in mobility can be attributed to the combined effect of doping in the

channel and reduced R_c of the S/D region by the top Al₂O₃ layer. A wafer-scale fabrication (Fig. 2F, inset photograph) of top-gated TFTs resulted in the excellent device yields (>95%), long-term stability (fig. S11), and high uniformity in switching parameters; most of the TFTs showed the high-mobility values (17 to 20 cm² V⁻¹ s⁻¹), low hysteresis (<0.75 V), high ON/OFF ratio (>10⁶), and positive V_{th} (5 ± 2 V) (Fig. 2F and fig. S8). Thus, highly reliable and uniform performances of top-gated TFTs render them suitable for use as the backplane of OLED displays.

The performance of a single-OLED pixel connected with a bilayer MoS₂ TFT before the operation of the large-area AM-OLED display was examined (Fig. 3, A and B, and fig. S12). The current density followed the diode characteristics; this observation is evident as OLEDs inherently behave as diodes. The turn-on voltage at 10 cd m⁻² was 4 V. The luminance linearly increased and reached ≥ 5000 cd m⁻² at a voltage greater than 8 V, indicating the excellent emissivity of the fabricated OLED (33). The OLED operation was tested by the application of voltage to drive TFT. The representative OLED exhibited excellent emission upon the application of V_{Gate} of approximately 8 V and V_{Data} of approximately 9 V to the gate and drain terminals of the driving TFT, respectively (Fig. 3C). Moreover, with a unit increase in V_{Gate} (4 to 9 V) at a constant V_{Data} of approximately 9 V, the emission intensity of the OLED was distinguishable (Fig. 3D). At V_{Gate} of 9 V, the maximum luminance reached 408 cd m⁻²; this value is sufficient for display applications, indicating that the fabricated MoS₂ TFT is capable of driving the OLED (33). Figure 3E shows the increase in the OLED current (I_{OLED}) against the data bias V_{Data} at different values of V_{Gate} . The value of I_{OLED} in the OFF state remained stable, indicating a leakage-free operation of the driving TFT, whereas, in the ON state, it significantly increased with V_{Gate} . The OLED requires a minimum threshold voltage to turn ON owing to its diode-like behavior. At a low V_{Data} (<5 V), the OLED was turned OFF; therefore, I_{OLED} is independent of V_{Gate} . In

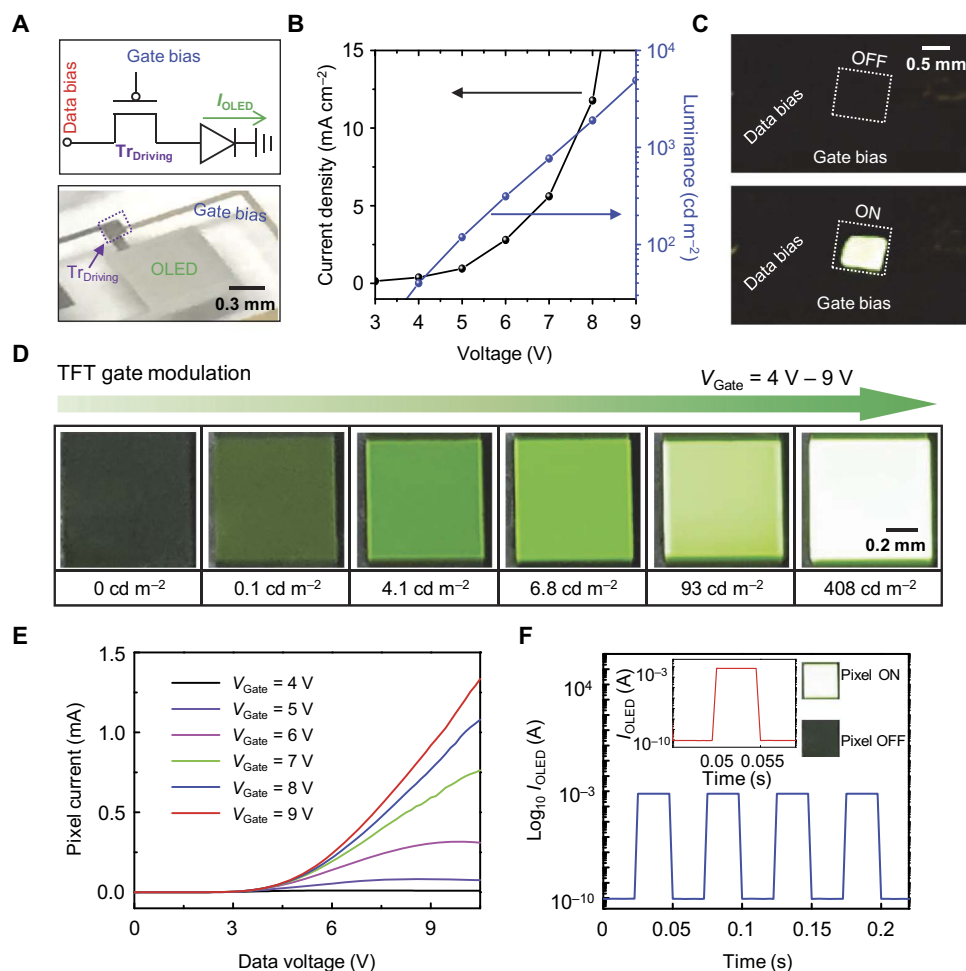


Fig. 3. The device characteristics of an OLED pixel driven by MoS₂ TFT. (A) Equivalent circuit diagram (top) and optical image of unit AM-OLED pixel by a single TFT. The single pixel is composed of a transistor and diode for a demonstration of the simplified active-matrix circuitry. (B) Current density and luminance of typical OLED device as a function of applying voltage. (C) Photographic images of ON/OFF switching using gate bias control of MoS₂ TFT. (D) Brightness control of unit OLED pixel according to gate bias. Luminance is well distinguishable as a function of the bias, which is stepped from 4 to 9 V (steps, 1 V). (E) Current-voltage (*I*-*V*) characteristics of the unit pixel during data voltage sweep from 0 to 10 V with gate bias steps. (F) Plot of pixel switching properties controlled using gate bias repeatedly. OLED is reliably turned ON and OFF using the MoS₂ TFT gate signal.

contrast, it turned ON at high $V_{\text{Data}} (\geq 5 \text{ V})$; thus, I_{OLED} significantly increased with V_{Data} (fig. S13) and demonstrated an apparent V_{Gate} dependency. The OLED exhibited rapid ON and OFF states against a repeated V_{Gate} pulse of $\pm 10 \text{ V}$ (Fig. 3F). The response time was estimated to be 2.5 ms, which was limited by the measurement system, but was still sufficiently low to drive the OLED with a short delay time (3). All the aforementioned operations of single OLEDs driven by the MoS₂ TFT indicated that the MoS₂ TFT in the developed top-gate configuration successfully drove the OLED unit.

The prototype ultrathin flexible AM-OLED display driven by a bilayer MoS₂-based backplane was demonstrated. The complete assembly (inset of Fig. 4A and fig. S14), including the active-matrix array and deposited OLED units, was arranged on a thin PET sheet (thickness, 6 μm) with the help of polydimethylsiloxane-coated glass carrier substrate (fig. S15). The representative AM-OLED exhibited a thickness of approximately 7 μm , which is thin enough to yield a smaller value of bending stiffness. The MoS₂-based backplane contributes significantly to the realization of a low value of bending stiffness owing to the good mechanical property of the atomically thin MoS₂ layer. Thus, a low

value of bending stiffness of resulting device facilitates conformal contact to human skin, and the excellent mechanical endurance of MoS₂ allows the good operation of the device after the attachment (Fig. 4A). The current ON/OFF mapping corresponding to a representative letter “M” showed that all the pixels (6×6 array) functioned well with the variation of ON/OFF current ($\pm 2\%$) without any external compensation circuits, indicating the excellent control of the active matrix on the OLED units (Fig. 4B). The AM-OLED display demonstrated a stable performance during continuous operation while being attached to a human wrist (movie S1 and snapshots in Fig. 4C). Four alphanumeric characters—“M,” “O,” “S,” and “2”—were displayed with rapid response to the systematic change of the program codes for each character and real-time control of V_{Gate} and V_{Data} . The AM-OLED display also functioned well without device failure when it was peeled from the carrier glass substrate (movie S2 and Fig. 4D). Furthermore, the AM-OLED display exhibited excellent endurance under repeated bending tests with a bending radius of 0.7 mm, showing small current variation within 10% (fig. S16) (34). These small variations in the pixel current were recovered in a flat condition and did not affect the display

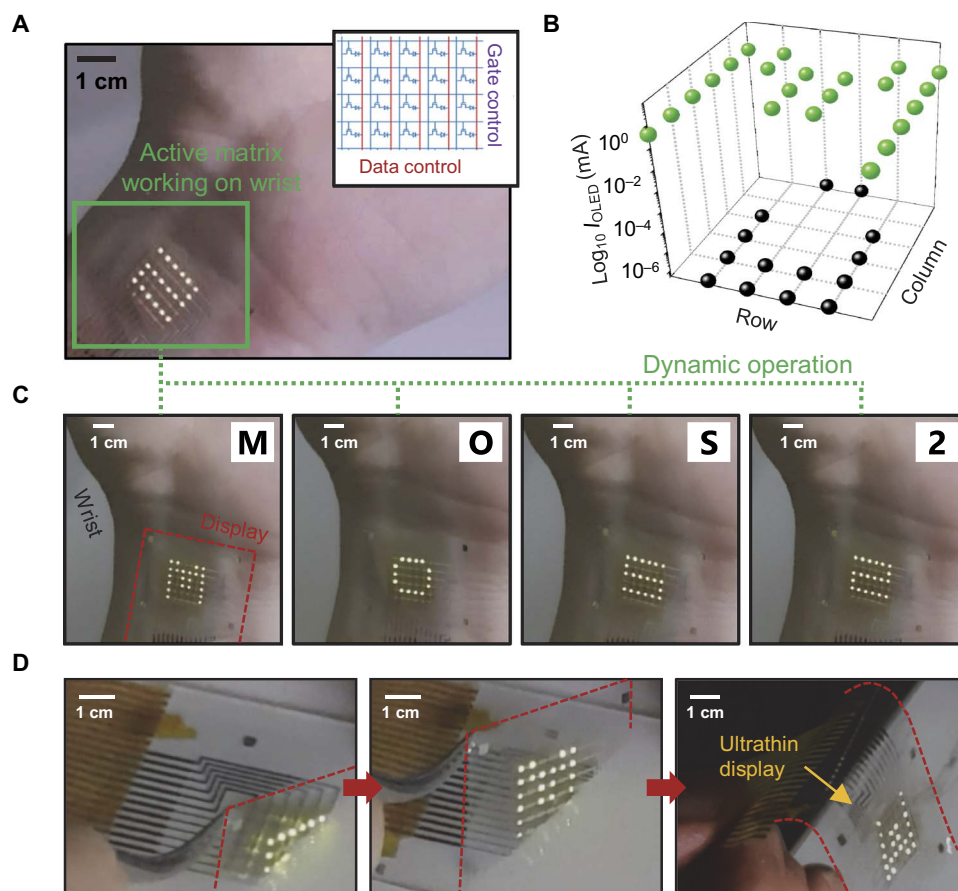


Fig. 4. Flexible OLED display driven by MoS₂ backplane circuitry. (A) Photographic image of ultrathin AM-OLED display on the human wrist while the display is operated; display stably attached to the skin owing to the ultrathin substrate. (B) Current mapping result during the display of the letter “M”; current of ON pixel (green dot) and OFF pixel (black dot), demonstrating uniform and low cross-talk properties. (C) Optical images of dynamic operation on human wrist using the external circuit; representative letters “M,” “O,” “S,” and “2” are sequentially changed on skin according to the active-matrix line addressing. (D) Optical images of the peel-off process from carrier glass substrate. The ultrathin display is folded during peel-off, owing to the low bending stiffness of the total display system.

operation. The excellent flexibility of the AM-OLED could be realized owing to the low bending stiffness of the entire AM-OLED assembly.

DISCUSSION

We demonstrated ultrathin flexible OLED displays driven by an active-matrix backplane circuitry composed of MoS₂-based TFTs. The improvement of device properties of TFT was realized by combining the n-type doping of MoS₂ at the S/D and channel regions, damping the Coulomb scattering, and reducing the trap charges and interface scattering through the modified TFT structure with a channel sandwiched between two Al₂O₃ layers. These MoS₂-based TFT arrays were successfully integrated with OLEDs on an ultrathin polymer substrate to demonstrate 6 × 6 active-matrix configurations. The brightness of each pixel was steadily adjusted from 0 to 408 cd m⁻² via the gate control of the MoS₂-based backplane circuitry, and the uniformity of display was confirmed by the ON/OFF current mapping with fast switching response properties. The flexible AM-OLED display was compatible even in a highly deformed state because it was well operated during the peel-off from the carrier substrate. The results reported here form the basis for the implantation of display-based applications on human movable body parts for wearable health-monitoring electronics, which advance the 2D material-based applications.

MATERIALS AND METHODS

Synthesis of MoS₂

Bilayer MoS₂ was grown using MOCVD. A 4-inch Si wafer with thermally grown 300-nm-thick SiO₂ was placed in a quartz tube with a diameter of 4.3 inch. Before the growth of MoS₂, the wafer was cleaned with water, acetone, and finally isopropanol. Molybdenum hexacarbonyl (MHC; 577766, Sigma-Aldrich) and dimethyl sulfide (DMS; 471577, Sigma-Aldrich), with high equilibrium vapor pressure, were chosen as the Mo and S precursors, respectively, and introduced into the quartz tube using H₂ and Ar as the carrier gases in the gas phase. The optimized parameters for the growth of bilayer MoS₂ included the pressure of 7.5 torr, growth temperature of 550°C, growth time of 20 hours, MHC flow of 1.0 standard cubic centimeter per minute (sccm), DMS flow of 0.3 sccm, Ar flow of 300 sccm, and H₂ flow of 10 sccm.

Fabrication and characterization of MoS₂ TFT

A 50-nm-thick bottom Al₂O₃ layer was deposited on a 300-nm-thick SiO₂ wafer using an atomic layer deposition (ALD) system. S/D electrodes (Cr/Au, 3/30 nm) were patterned on the Al₂O₃/SiO₂ wafer using general photolithography (W/L, 300/4 μm). The bilayer MoS₂ film was transferred onto the wafer and patterned as a channel via reactive ion etching using CHF₃/O₂ plasma. Subsequently, a 50-nm-thick top

Al₂O₃ dielectric layer was deposited on MoS₂. To avoid H₂O molecule traps and the formation of Mo–O bonds during the initial growth cycles of ALD, which significantly degrade the MoS₂ TFT performances, a possible combination of minimum H₂O exposure with low temperature was optimized. In addition, to improve the Al₂O₃/MoS₂ interface, the devices were baked at 110°C overnight under vacuum condition (35). Finally, the top-gate electrode (Cr/Au, 3/30 nm) was formed using photolithography and a lift-off process. MoS₂ TFT was characterized using a SourceMeter unit (Keithley 4200 SCS parameter analyzer, Keithley Instruments Inc.).

Fabrication of OLED

The ITO-coated substrate was used to fabricate the Green OLEDs. Prior to it, the substrate was cleaned using acetone, isopropyl alcohol, and deionized water, sequentially followed by drying and exposure to ultraviolet/ozone treatment for 15 min. Subsequently, layers of *N*, *N'*-di(1-naphthyl)-*N*, *N'*-diphenyl-(1,10-biphenyl)-4, 40-diamine (40 nm), tris-(8-hydroxy-quinoline) aluminum (Alq₃, 30 nm), 2, 3, 6, 7-tetrahydro-1, 1, 7, 7-tetramethyl-1H,5H,11H-10-(2-benzothiazolyl)quinolizine [9,9a,1gh] coumarin (5% doping), bathocuproine (5 nm), and Alq₃ (25 nm) were deposited as the hole transport layer, emitting layer, hole-blocking layer, and electron transport layer under vacuum of approximately 2×10^{-6} Torr at a deposition rate of 1 Å/s. Finally, LiF (1 nm) and Al (100 nm) layers were thermally deposited.

SUPPLEMENTARY MATERIALS

Supplementary material for this article is available at <http://advances.sciencemag.org/cgi/content/full/4/4/eaas8721/DC1>

Supplementary Text

fig. S1. Atomic force microscopy images of SiO₂ and Al₂O₃/SiO₂.

fig. S2. Cross-sectional transmission electron microscopy image of Al₂O₃/MoS₂/Al₂O₃ sandwiched structure.

fig. S3. Optical analysis of MoS₂ film on Al₂O₃ layer.

fig. S4. Optical analysis of MoS₂ film by Al₂O₃ layer encapsulation.

fig. S5. Optical analysis of MoS₂ film sandwiched with Al₂O₃ layer.

fig. S6. Schematic band diagram of Au/MoS₂ contacts with and without Al₂O₃ encapsulation.

fig. S7. Hysteresis of top-gated bilayer MoS₂ TFTs on SiO₂/Si substrate (green) and Al₂O₃/SiO₂/Si substrate (blue).

fig. S8. Statistical data analysis of electrical properties of modified MoS₂ TFT.

fig. S9. Electrical properties of single-crystal MoS₂ TFTs.

fig. S10. Contact and channel sheet resistance analysis of top-gated MoS₂ TFT.

fig. S11. The stability of Al₂O₃-encapsulated MoS₂ TFTs for 1-month period.

fig. S12. Intrinsic OLED properties and structure information.

fig. S13. Analysis of current-voltage characteristics of AM-OLED pixel at different gate biases from 4 to 9 V.

fig. S14. Layout structure of designed active-matrix display.

fig. S15. Schematic illustration of steps for ultrathin AM-OLED display fabrication.

fig. S16. Normalized ON current values of unit pixel at the initial bending radius of 0.7 mm repeatedly.

table S1. The characteristics of MoS₂-based TFTs with different device structures.

movie S1. Active-matrix display operation on human wrist with external circuit.

movie S2. The dynamic operation of ultrathin display during peeling-off process.

Reference (36)

REFERENCES AND NOTES

- M. Kaltenbrunner, T. Sekitani, J. Reeder, T. Yokota, K. Kuribara, T. Tokuhara, M. Drack, R. Schwödiauer, I. Graz, S. Bauer-Gogonea, S. Bauer, T. Someya, An ultra-lightweight design for imperceptible plastic electronics. *Nature* **499**, 458–463 (2013).
- T. Yokota, P. Zalar, M. Kaltenbrunner, H. Jinno, N. Matsuhisa, H. Kitanosako, Y. Tachibana, W. Yukita, M. Koizumi, T. Someya, Ultraflexible organic photonic skin. *Sci. Adv.* **2**, e1501856 (2016).
- M. Choi, B. Jang, W. Lee, S. Lee, T. W. Kim, H.-J. Lee, J.-H. Kim, J.-H. Ahn, Stretchable active matrix inorganic light-emitting diode display enabled by overlay-aligned roll-transfer printing. *Adv. Funct. Mater.* **27**, 1606005 (2017).
- K. Takei, T. Takahashi, J. C. Ho, H. Ko, A. G. Gillies, P. W. Leu, R. S. Fearing, A. Javey, Nanowire active-matrix circuitry for low-voltage macroscale artificial skin. *Nat. Mater.* **9**, 821–826 (2010).
- B. C.-K. Tee, A. Chortos, A. Berndt, A. K. Nguyen, A. Tom, A. McGuire, Z. C. Lin, K. Tien, W.-G. Bae, H. Wang, P. Mei, H.-H. Chou, B. Cui, K. Deisseroth, T. N. Ng, Z. Bao, A skin-inspired organic digital mechanoreceptor. *Science* **350**, 313–316 (2015).
- D.-H. Kim, N. Lu, R. Ma, Y.-S. Kim, R.-H. Kim, S. Wang, J. Wu, S. M. Won, H. Tao, A. Islam, K. J. Yu, T.-i. Kim, R. Chowdhury, M. Ying, L. Xu, M. Li, H.-J. Chung, H. Keum, M. McCormick, P. Liu, Y.-W. Zhang, F. G. Omenetto, Y. Huang, T. Coleman, J. A. Rogers, Epidermal electronics. *Science* **333**, 838–843 (2011).
- W. Gao, S. Emaminejad, H. Y. Y. Nyein, S. Challa, K. Chen, A. Peck, H. M. Fahad, H. Ota, H. Shiraki, D. Kiriya, D.-H. Lien, G. A. Brooks, R. W. Davis, A. Javey, Fully integrated wearable sensor arrays for multiplexed in situ perspiration analysis. *Nature* **529**, 509–514 (2016).
- J. Liang, L. Li, X. Niu, Z. Yu, Q. Pei, Elastomeric polymer light-emitting devices and displays. *Nat. Photonics* **7**, 817–824 (2013).
- J. Wang, C. Yan, K. J. Chee, P. S. Lee, Highly stretchable and self-deformable alternating current electroluminescent devices. *Adv. Mater.* **27**, 2876–2882 (2015).
- M. A. McCarthy, B. Liu, E. P. Donoghue, I. Kravchenko, D. Y. Kim, F. So, A. G. Rinzler, Low-voltage, low-power, organic light-emitting transistors for active matrix displays. *Science* **332**, 570–573 (2011).
- S. Ju, J. Li, J. Liu, P.-C. Chen, Y.-g. Ha, F. Ishikawa, H. Chang, C. Zhou, A. Facchetti, D. B. Janes, T. J. Marks, Transparent active matrix organic light-emitting diode displays driven by nanowire transistor circuitry. *Nano Lett.* **8**, 997–1004 (2008).
- J. Zhang, Y. Fu, C. Wang, P.-C. Chen, Z. Liu, W. Wei, C. Wu, M. E. Thompson, C. Zhou, Separated carbon nanotube macroelectronics for active matrix organic light-emitting diode displays. *Nano Lett.* **11**, 4852–4858 (2011).
- F. Bonaccorso, Z. Sun, T. Hasan, A. C. Ferrari, Graphene photonics and optoelectronics. *Nat. Photonics* **4**, 611–622 (2010).
- G.-H. Lee, Y.-J. Yu, X. Cui, N. Petrone, C.-H. Lee, M. S. Choi, D.-Y. Lee, C. Lee, W. J. Yoo, K. Watanabe, T. Taniguchi, C. Nuckolls, P. Kim, J. Hone, Flexible and transparent MoS₂ field-effect transistors on hexagonal boron nitride-graphene heterostructures. *ACS Nano* **7**, 7931–7936 (2013).
- K. Kang, S. Xie, L. Huang, Y. Han, P. Y. Huang, K. F. Mak, C.-J. Kim, D. Muller, J. Park, High-mobility three-atom-thick semiconducting films with wafer-scale homogeneity. *Nature* **520**, 656–660 (2015).
- M. Park, Y. J. Park, X. Chen, Y.-K. Park, M.-S. Kim, J.-H. Ahn, MoS₂-based tactile sensor for electronic skin applications. *Adv. Mater.* **28**, 2556–2562 (2016).
- S. Yu, J. S. Kim, P. J. Jeon, J. Ahn, J. C. Park, S. Im, Transition metal dichalcogenide-based transistor circuits for gray scale organic light-emitting displays. *Adv. Funct. Mater.* **27**, 1603682 (2017).
- J. S. Kim, P. J. Jeon, J. Lee, K. Choi, H. S. Lee, Y. Cho, Y. T. Lee, D. K. Hwang, S. Im, Dual gate black phosphorus field effect transistors on glass for NOR logic and organic light emitting diode switching. *Nano Lett.* **15**, 5778–5783 (2015).
- J. Zhang, H. Yu, W. Chen, X. Tian, D. Liu, M. Cheng, G. Xie, W. Yang, R. Yang, X. Bai, D. Shi, G. Zhang, Scalable growth of high-quality polycrystalline MoS₂ monolayers on SiO₂ with tunable grain sizes. *ACS Nano* **8**, 6024–6030 (2014).
- A. Allain, J. Kang, K. Banerjee, A. Kis, Electrical contacts to two-dimensional semiconductors. *Nat. Mater.* **14**, 1195–1205 (2015).
- H. Yabuta, M. Sano, K. Abe, T. Aiba, T. Den, H. Kumomi, K. Nomura, T. Kamiya, H. Hosono, High-mobility thin-film transistor with amorphous InGaZnO₄ channel fabricated by room temperature rf-magnetron sputtering. *Appl. Phys. Lett.* **89**, 112123 (2006).
- H. E. A. Huitema, G. H. Gelinck, J. B. P. H. van der Putten, K. E. Kuijk, C. M. Hart, E. Cantatore, P. T. Herwig, A. J. J. M. van Breemen, D. M. de Leeuw, Plastic transistors in active-matrix displays. *Nature* **414**, 599 (2001).
- A. D. Franklin, Nanomaterials in transistors: From high-performance to thin-film applications. *Science* **349**, aab2750 (2015).
- C. Wang, D. Hwang, Z. Yu, K. Takei, J. Park, T. Chen, B. Ma, A. Javey, User-interactive electronic skin for instantaneous pressure visualization. *Nat. Mater.* **12**, 899–904 (2013).
- A. Valsaraj, J. Chang, A. Rai, L. F. Register, S. K. Banerjee, Theoretical and experimental investigation of vacancy-based doping of monolayer MoS₂ on oxide. *2D Mater.* **2**, 045009 (2015).
- D. Jena, A. Konar, Enhancement of carrier mobility in semiconductor nanostructures by dielectric engineering. *Phys. Rev. Lett.* **98**, 136805 (2007).
- Y. Cui, R. Xin, Z. Yu, Y. Pan, Z.-Y. Ong, X. Wei, J. Wang, H. Nan, Z. Ni, Y. Wu, T. Chen, Y. Shi, B. Wang, G. Zhang, Y.-W. Zhang, X. Wang, High-performance monolayer WS₂ field-effect transistors on high-κ dielectrics. *Adv. Mater.* **27**, 5230–5234 (2015).
- M. S. White, M. Kaltenbrunner, E. D. Glowacki, K. Gutnichenko, G. Kettlgruber, I. Graz, S. Aazou, C. Ulbricht, D. A. M. Egbe, M. C. Miron, Z. Major, M. C. Scharber, T. Sekitani, T. Someya, S. Bauer, N. S. Sariciftci, Ultrathin, highly flexible and stretchable PLEDs. *Nat. Photonics* **7**, 811–816 (2013).
- D. Kiriya, M. Tosun, P. Zhao, J. S. Kang, A. Javey, Air-stable surface charge transfer doping of MoS₂ by benzyl viologen. *J. Am. Chem. Soc.* **136**, 7853–7856 (2014).

30. A. Sanne, R. Ghosh, A. Rai, H. C. P. Movva, A. Sharma, R. Rao, L. Mathew, S. K. Banerjee, Top-gated chemical vapor deposited MoS₂ field-effect transistors on Si₃N₄ substrates. *Appl. Phys. Lett.* **106**, 062101 (2015).
31. J. Chen, W. Tang, B. Tian, B. Liu, X. Zhao, Y. Liu, T. Ren, W. Liu, D. Geng, H. Y. Jeong, H. S. Shin, W. Zhou, K. P. Loh, Chemical vapor deposition of high-quality large-sized MoS₂ crystals on silicon dioxide substrates. *Adv. Sci.* **3**, 1500033 (2016).
32. W. S. Leong, X. Luo, Y. Li, K. H. Khoo, S. Y. Quek, J. T. L. Thong, Low resistance metal contacts to MoS₂ devices with nickel-etched-graphene electrodes. *ACS Nano* **9**, 869–877 (2015).
33. T. Sekitani, H. Nakajima, H. Maeda, T. Fukushima, T. Aida, K. Hata, T. Someya, Stretchable active-matrix organic light-emitting diode display using printable elastic conductors. *Nat. Mater.* **8**, 494–499 (2009).
34. S. Manzeli, A. Allain, A. Ghadimi, A. Kis, Piezoresistivity and strain-induced band gap tuning in atomically thin MoS₂. *Nano Lett.* **15**, 5330–5335 (2015).
35. J.-G. Song, S. J. Kim, W. J. Woo, Y. Kim, I.-K. Oh, G. H. Ryu, Z. Lee, J. H. Lim, J. Park, H. Kim, Effect of Al₂O₃ deposition on performance of top-gated monolayer MoS₂-based field effect transistor. *ACS Appl. Mater. Interfaces* **8**, 28130–28135 (2016).
36. J. Jeon, S. K. Jang, S. M. Jeon, G. Yoo, Y. H. Jang, J.-H. Park, S. Lee, Layer-controlled CVD growth of large-area two-dimensional MoS₂ films. *Nanoscale* **7**, 1688–1695 (2015).

Acknowledgments

Funding: This work was supported by the National Research Foundation of Korea (NRF-2015R1A3A2066337). **Author contributions:** J.-H.A. planned and supervised the project. S.Y.K. co-supervised the project. B.K.S. advised and supported the project. M.C. and Y.J.P. conducted most of the experiments regarding the device fabrication and characterization. S.-R.B. interpreted the data and supported OLED part experiment. All authors analyzed the data and wrote the manuscript. **Competing interests:** J.-H.A. and Y.J.P. are inventors on a Korean patent application related to this work filed by Yonsei University (10-2017-0055578, 28 April 2017). The authors declare no other competing interests. **Data and materials availability:** All data needed to evaluate the conclusions in the paper are present in the paper and/or the Supplementary Materials. Additional data related to this paper may be requested from the authors.

Submitted 28 December 2017

Accepted 2 March 2018

Published 20 April 2018

10.1126/sciadv.aas8721

Citation: M. Choi, Y. J. Park, B. K. Sharma, S.-R. Bae, S. Y. Kim, J.-H. Ahn, Flexible active-matrix organic light-emitting diode display enabled by MoS₂ thin-film transistor. *Sci. Adv.* **4**, eaas8721 (2018).